Experimental Ultra Wideband Path Loss Models for Implant Communications

C. Garcia-Pardo, A. Fornes-Leal and N. Cardona
Universitat Politècnica de València, iTEAM
46022 Valencia,
{cgpardo, alforlea, ncardona}@iteam.upv.es

R. Chávez-Santiago, J. Bergsland, I. Balasingham
The Intervention Centre, Oslo University Hospital,
NO-0027 Oslo, Norway
jacobbergsland622@ googlemail.com;
ilangko.balasingham@medisin.uio.no

S. Brovoll, Ø. Aardal and S.-E. Hamran
The Norwegian Defence Research Establishment (FFI),
NO-2027 Kjeller, Norway
{Sverre.Brovoll, Oyvind.Aardal,
Svein-Erik.Hamran}@ffi.no

R. Palomar
The Intervention Centre,
Oslo University Hospital.
Postboks 4950, 0424 Oslo, Norway.

***Abstract*—Ultra wideband (UWB) signals possess characteristics that may enable high data rate communications with deeply implanted medical sensors and actuators. Nevertheless, this application could be hindered in part by international spectrum regulations, which restrict UWB communications to 3.1-10.6 GHz where propagation conditions through the human body are rather unfavorable. Therefore, for the proper feasibility assessment and design of implant communications using UWB signals, accurate models of the radio channel are of utmost importance. Hence, we present UWB path loss models for the two most commonly used implant communication scenarios, i.e., in-body to on-body (IB2OB) and in-body to off-body (IB2OFF). These models were extracted from in vivo measurements in the abdominal cavity within 3.1-8.5 GHz using a living porcine subject. A thorough comparison between this modeling approach and channel measurements using a homogeneous phantom, which mimics the electromagnetic behaviour of muscle tissue, is presented too. Measurements in a homogeneous propagation medium are simpler to perform, but they fail to capture several physiological effects observed in a living subject. Thus, we measured the deviation between the phantom-based and in-vivo-based path loss models. In general, phantom measurements yielded a more pessimistic estimation of the path loss. We provide the correction factors to adjust easy-to-perform phantom-based measurements to more realistic path loss values, which can assist the biomedical engineer in the early stages of design and testing of wireless implantable devices.**

Keywords—*channel model, implant, in vivo, path loss, phantom.*

I. INTRODUCTION

The utilization of wireless technologies for a variety of medical applications has increased dramatically in the last years. Significant advances in microelectronics have enabled the integration of biomedical sensors and radio transceivers into *wearable* and *implantable* wireless sensors. Such devices are crucial for the future implementation of inexpensive, continuous, and ambulatory monitoring of patients' physiological signals [1]. The IEEE Standard 802.15.6-2012 [2] allocates the different industrial, scientific, medical (ISM) frequency bands and other parts of the electromagnetic spectrum to the operation of *wearable* sensors. These include the spectrum of 3.1-10.6 GHz, which is for communications using ultra wideband (UWB) signals on the condition that some coexistence regulations are respected. According to the United States' Federal Communications Commission (FCC), UWB signals are those whose relative bandwidth is higher than the 20% of the center frequency, or whose absolute bandwidth is greater than 500 MHz. These signals have inherent properties that make them very convenient for the wireless interface with wearable biomedical sensors [3], and may not represent a threat to the patients' safety [4]. Moreover, UWB devices require ultra low power and low signal-to-noise ratio (SNR) using different modulation and coding schemes. All these characteristics are desirable for the radio interfaces with *implantable* sensors too, which currently are confined to the Medical Implant Communication Services (MICS) band by the IEEE Standard 802.15.6-2012. The MICS band operates from 402 to 405 MHz so it presents a relatively good propagation behaviour and enables the use of reasonable-size antennas, but its limited bandwidth constrains the communication links to low data transmission rates only [5]. On the other hand, the feasibility of high data rate transmissions in implant scenarios using UWB has been demonstrated through various computer simulations and physical experiments, e.g., [6]-[9], albeit different transmission rates in each case. For instance, computer simulations in [6] predicted the feasibility of transmitting up to

This work was supported by the European COST Action IC1004 through two Short-Term Scientific Missions (reference no. COST-STSM-IC1004-17489 and -21376). The work of R. Chávez-Santiago and I. Balasingham was supported by the Research Council of Norway through the MELODY Project-Phase II (contract no. 225885). The work of C. Garcia-Pardo, A. Fornes-Leal and N. Cardona was supported by the Ministerio de Educación y Ciencia, Spain (TEC2014-60258-C2-1-R), by the European FEDER funds.

100 Mbit/s for UWB implant communications. A subsequent *in vivo* experiment on a living porcine subject demonstrated a much lower data rate of 1 Mbit/s using an UWB link for a maximal implantation depth of 12 cm and a bit error rate (BER) of 10^{-2} [9]. Hence, it is evident that more research is needed to verify whether a deeply implanted sensor can actually communicate at such high data rates. The large attenuation suffered by UWB signals when are propagated through biological tissues is the main hindering factor. Therefore, accurate modeling of the communication channel is of utmost importance for the feasibility assessment and design of implant communication systems using UWB signals.

However, only a few attempts to model the UWB implant radio channel have been reported, e.g., [10]-[13]. Most of these path loss models were extracted from computer simulations using digital voxel anatomical models. Despite the accurate representation of the dielectric properties of the human body provided by such models, numerical simulations do not capture the effects of some physiological processes such as respiration, blood circulation, or temperature gradients. Hence, *in vivo* measurements using animals that anatomically resemble some parts of the human body have been suggested for a more accurate modeling of the UWB implant channel [5]. However, such measurements are expensive and require the use of an operating room with all the necessary medical staff and governmental approval for the experimental implantation of the antennas. To the best of our knowledge, the sole UWB path loss model for implant communications derived from measurements in living swine was reported in [14]. Nevertheless, the implantable antenna used for the measurements therein was optimized to radiate within 3.1-4.8 GHz [15], whereas the channel measurements were conducted for 1-6 GHz. A compensation of the return loss (S_{11} parameter) of the antenna was performed in order to cover and model the entire 1-6 GHz frequency band. This mathematical manipulation, however, inevitably resulted in uncertainty about the accuracy of the path loss estimation.

Thus, in this paper we present some UWB path loss models extracted from *in vivo* channel measurements using a living porcine subject and an implantable antenna covering the entire 3.1-10.6 GHz frequency band. The two most commonly used implant communication scenarios, namely in-body to on-body (IB2OB) and in-body to off-body (IB2OFF), were characterized within 3.1-5 GHz and 3.1-8.5 GHz, respectively. We also conducted measurements using a muscle-mimicking phantom (i.e., a chemical solution that provides the dielectric properties of muscle tissue) for the same frequency bands and scenarios, and with the same antennas. The rationale was the fact that phantom-based measurements are easier to perform in a laboratory. However, because of the homogeneity of a phantom the effects of a highly inhomogeneous geometry of the propagation medium (as in the human body) are ignored, leading to an inaccurate estimation of the path loss. By comparing our two modeling approaches, we provide a quantitative estimation of the deviation between phantom-based and *in vivo* measurements, which allows adjusting easy-to-perform phantom measurements to path loss values that are more realistic.

The remainder of this paper is organized as follows. Section II describes our methodology to perform *in vivo* and phantom-based measurements. Section III presents the extracted path loss models. Section IV summarizes our conclusions.

II. Measurement Setup And Methodology

A. Propagation Scenarios

For the set of *in vivo* measurements, the two most commonly used scenarios for implant communications were considered, i.e.:

- *In-Body to On-Body* (IB2OB): one antenna was implanted into the swine's abdominal cavity whereas the second antenna was on its skin.
- *In-Body to Off-Body* (IB2OFF): one antenna was implanted into the swine's abdominal cavity whereas the second antenna was located in the air several centimeters from its skin.

These scenarios were also mimicked for the phantom-based measurements, although some adjustments had to be done to adapt them to the geometry of the phantom. Below, the measurement setups for the two measurement approaches, i.e., *in vivo* and phantom, are described in detail.

B. In Vivo Measurements Setup

The *in vivo* measurements were performed at the Intervention Centre, Oslo University Hospital, with the approval of the Norwegian Animal Research Authority (NARA). A Norwegian landrace female pig with body weight of 46 kg was utilized because its size was deemed appropriate to approximate the anatomy of an average human torso. The measurement setup particularized for the IB2OB scenario is shown in Fig. 1.

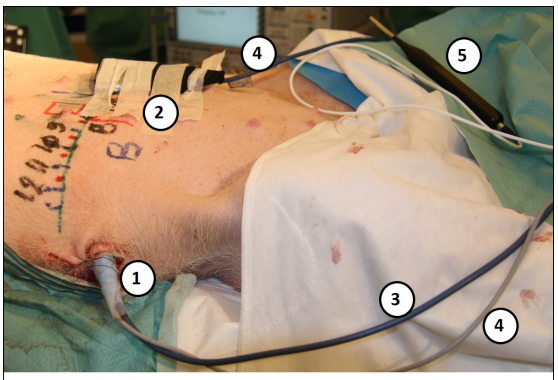

Fig. 1. *In vivo* measurement setup for the IB2OB scenario.

For the IB2OB case, one antenna was implanted into the

swine's abdominal cavity through laparotomy and was fixed at an implantation distance d_{in}=3.5 cm from a reference point on top of the abdomen. The other antenna was placed on the swine's skin. The antennas were connected to a vector network analyzer (VNA) with a maximal operation frequency of 8.5 GHz. The frequency responses of the coaxial cables connecting the antennas to the VNA were subtracted from the channel measurements by through calibration. The distance separating the antennas was measured with an electromagnetic tracking system (NDI Aurora®), which provided an RMS error margin of 0.7 mm.

For the IB2OFF case, an external antenna was mounted on a tripod and located at a distance d_{off} from the swine's skin. For clarity, the measured locations of the antennas for each scenario are sketched in Fig. 2, where d_{in} is the aforementioned reference implantation distance.

Thus, from Fig. 2, the distance between the two antennas, d, took the different values d_1, d_2, d_3, …, d_n for the IB2OB scenario, and d_{in}+d_{off} for IB2OFF.

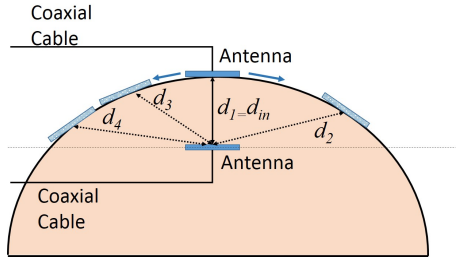

(a) IB2OB

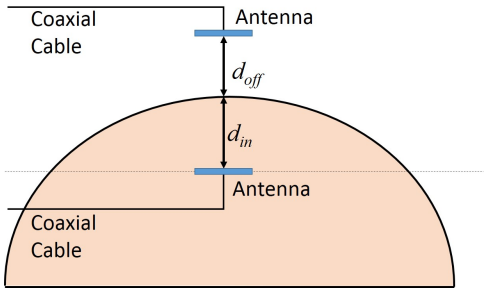

(b) IB2OFF

Fig. 2. Antenna locations for the *in vivo* measuments.

C. Phantom-Based Measurements Setup

An aqueous solution of sucrose ($C_{12}H_{22}O_{11}$/1.0 M) was prepared, which reportedly approximates well the complex permittivity of the human muscle tissue within 3.1-10.6 GHz [16]. The solution was contained in a Styrofoam™ cube of 22×22×16 cm^3. The locations of the antennas for each scenario in the phantom are depicted in Fig. 3.

For the IB2OB scenario, one antenna was submerged in the aqueous solution, whereas the second antenna was located on the external wall of the cube container as shown in Fig. 3(a). The submerged antenna was placed at different locations inside the solution to simulate different implantation distances. For the IB2OFF scenario, the submerged antenna was fixed at a distance d_{in}=4 cm from the internal wall of the container, whereas the second antenna was moved away in the air as indicated in Fig. 3(b).

D. UWB Antennas

Two UWB patch antennas (see Fig. 4) that operate in the 3.1-10.6 GHz frequency band were used [17]. These antennas present an omnidirectional radiation pattern in the horizontal plane.

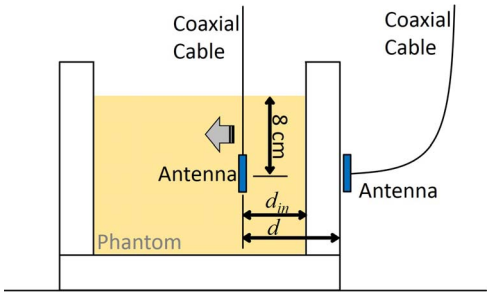

(a) IB2OB

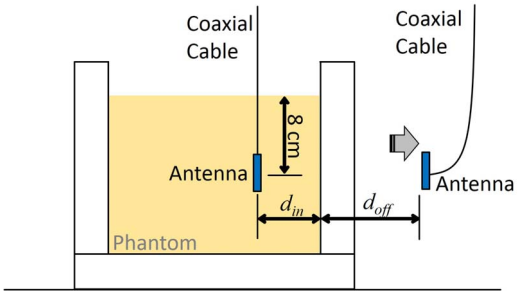

(b) IB2OFF

Fig. 3. Antenna locations for the phantom-based measurements.

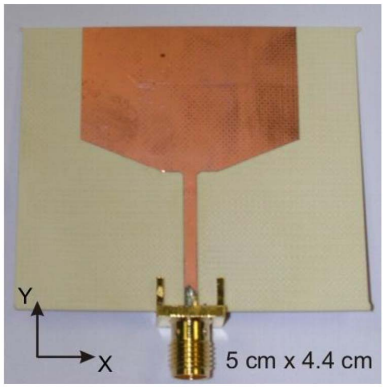

Fig. 4. UWB patch antenna used in the measurements.

Before the implantation or the immersion, the antenna was covered with a layer of nitrile butadiene rubber (NBR) to avoid the physical contact between the board elements or the antenna's connector; and the liquid phantom or the abdominal fluids resulting in a short-circuit.

Concerning the antenna matching, the S_{11} and S_{22} parameters were checked just before measurements after the NBR covering. A value below −10 dB was recorded in case of phantom immersion as well as in vivo implantation.

E. Measurement Methodology

The measurement methodology was based on the measurement of the S_{21} parameter from the VNA in the 3.1-8.5 GHz frequency band (the maximum operation frequency of the VNA was 8.5 GHz). N=20001 frequency points were measured resulting in a frequency resolution of Δf=270 kHz. The noise floor was–110 dBm for an intermediate frequency of $f_{\mathrm{IF}} = 3\,\mathrm{kHz}$. The output power was 10 dBm so that the dynamic range was enough to undertake the measurements. In order to improve the signal-to-noise ratio (SNR) of the measurements, k=5 snapshots of the channel were recorded. The S_{21} parameter was measured with identical configuration for different values of the distance between antennas, d, for both phantom and in vivo measurements.

After measurements, data were processed and analysed in Matlab™.

II. Results

From measurements, we obtained the $S_{21}(f,d,k)$ parameter, being f one of the $N = 20001$ frequency points, d the distance between antennas, and k the snapshot. Before measurement processing, the five snapshots were averaged, obtaining $\widetilde{S}_{21}(f,d)$. Hence, the relative received power as a function of distance for a certain distance between antennas can be computed as:

$$P(f,d_i) = \left|\tilde{S}_{21}(f,d_i)\right|^2 \tag{1}$$

The mean path loss, $PL(d_i)$, can be deduced from $P(f,d_i)$ by computing the expectation $E_f\{\ \}$ over all the frequency points in the entire frequency band as:

$$PL(d_i) = -10\log_{10}\left(E_f\left\{P(f,d_i)\right\}\right) \tag{2}$$

It should be highlighted, only those points above the noise floor were considered for the analysis.

A. In-Body to On-Body

From our measurements it was evident that only the lower part of the UWB spectrum was useful to extract an IB2OB model because of the high path loss suffered at higher frequencies as most of the path length was in a lossy medium. Thus, the mean path loss was computed for 3.1-5 GHz in order to consider only those values above the noise level. Above 5 GHz, most measurements in this case fell below the VNA's noise level. Fig. 5 shows the mean path loss extracted from *in vivo* and phantom-based measurements, respectively. For the phantom-based measurements, it should be noted that the distance between the two antennas in centimeters is:

$$d = d_{\mathrm{in}} + w_{\mathrm{th}} \tag{3}$$

where w_{th} is the phantom's wall thickness. However, after measuring the path loss through the 4 cm thick Styrofoam™ wall, it was found to be negligible, so it can be assumed that:

$$PL(d_{\mathrm{in}}) \approx PL(d) \tag{4}$$

Thus, in a real IB2OB situation where a wearable sensor is in direct contact with the skin, d_{in}=d, so that $PL(d_{\mathrm{in}})$= $PL(d)$.

Overestimation of the path loss in the phantom-based measurements can be observed, which increases with the distance separating the antennas. This effect was also observed in previous studies in [18], where the relative received power was lower in case of IB2OB *in vivo* measurements. This is explained by the detuning of the UWB phantom over the entire frequency band [16]. In particular, the loss factor of the phantom is higher than that of the muscle [19] in the UWB band and this discrepancy increases with frequency in the 3–5 GHz band. It should be mentioned that measurements for distances between 3 and 6 cm were performed in near-field conditions. However, in [20] authors determine that the use of the nonradiative near-field region of an implanted antenna can even improved the range of an in-body communication link.

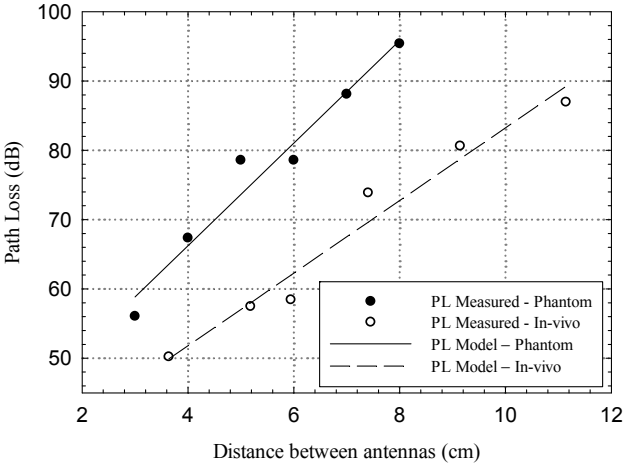

Fig. 5. IB2OB measured and modeled path loss within 3.1-5 GHz.

Regardless of this effect, the measured path loss in decibels for both cases can be modeled as a linear function of d in centimeters, i.e.:

$$PL(d) = PL_0 + \alpha d \tag{5}$$

where PL_0 is an initial path loss value in decibels observed in the limit when $d \to 0$, and α is a scaling factor. This model is valid for $3 \le d \le 11$ cm. The path loss model parameters for each case are presented in

TABLE I. Obviously, the values of PL_0 and α are larger for the phantom-based path loss model.

TABLE I
PATH LOSS MODEL PARAMETERS FOR IB2OB CHANNEL SCENARIO

	Phantom	*In Vivo*
PL_0 (dB)	36.6	30.8
α (dB/cm)	7.4	5.2

The path loss models above represent a practical tool for the assessment and design of implant communication systems using UWB signals. As mentioned before, channel measurements and transceiver tests can be performed more easily in phantoms. However, *in vivo* measurements using laboratory animals, specifically living swine, yield a good approximation to the performance of wireless implanted devices in the human torso as has been demonstrated in a number of experiments, e.g., [9], [21], [22]. The drawback of *in vivo* measurements is their high cost and difficulty to perform. Hence, using our results it is enough to simply add a correction factor to phantom measurements in order to obtain values that are more realistic. This correction factor is the difference between the corresponding phantom-based and *in vivo* path loss values for a given distance separating the antennas. From our measurements, the correction factor in decibels can be modeled as a linear function of the distance, $C(d)$, with a slope equal to 2.2 and a constant factor of 5.8 dB. This function and its corresponding mathematical expression are shown in Fig. 6.

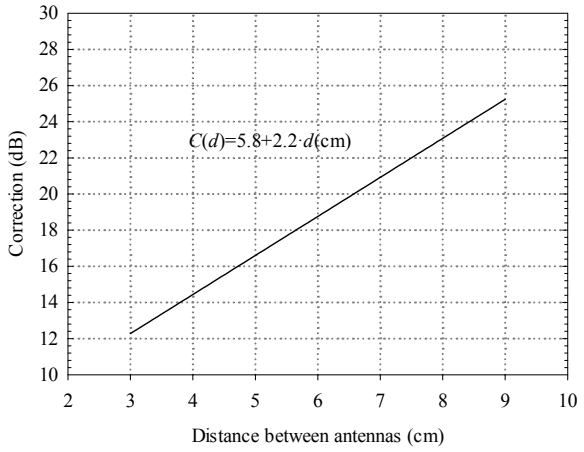

Fig. 6. Correction factor in decibels as a function of distance that can be applied to phantom-based measurements to fit *in vivo* measurements.

B. In-Body to Off-Body

As mentioned before, in the IB2OFF scenario the inner antenna was fixed at d_{in}=3.5cm while the outer antenna was moved away in the air (see Fig. 2(b) and Fig. 3(b)) during measurements. Hence, most of the propagation medium was the air resulting in a less lossy propagation path. Therefore, the measurements within the entire 3.1-8.5 GHz frequency band were useful to extract the IB2OFF path loss models. Fig. 7 shows the mean path loss as a function of the off-body distance (d_{off} in Fig. 3(b)) for both phantom-based and *in vivo* measurements.

As in the IB2OB scenario, the phantom-based measurements overestimated the path loss because of phantom detuning. Moreover, the difference in the path loss also increases with the distance from the skin, d_{off}. However, in this case the increment is caused by the different arrangement of the surrounding objects (furniture, equipment, etc.) of the operation room and laboratory where the *in vivo* and phantom-based measurements were performed, respectively.

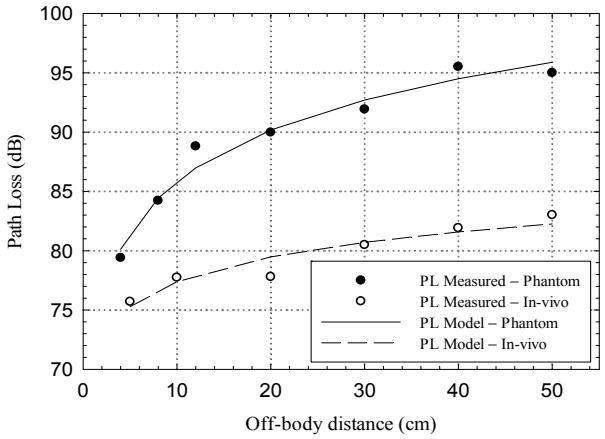

Fig. 7. IB2OFF measured and modeled path loss within 3.1-8.5 GHz.

Here, the measured path loss in decibels can be modeled as a log-distance linear function of d in centimeters for both cases, i.e.:

$$PL(d_{\text{off}}) = PL_0 + 10\gamma \log_{10}\left(\frac{d_{\text{off}}}{d_{\text{ref}}}\right) \quad (6)$$

where γ is a path loss exponent, PL_0 is an initial path loss value in decibels deduced in the limit when the off-body distance tends to $d_{\text{ref}} \rightarrow 1$. This model is valid for $4 \leq d_{\text{off}} \leq 50$ cm. TABLE II shows the model parameters for the *in vivo* and phantom-based measurements, respectively.

TABLE II
PATH LOSS MODEL PARAMETERS FOR IB2OFF CHANNEL SCENARIO

	Phantom	*In Vivo*
PL_0 (dB)	71.5	70.4
γ	1.4	0.7

Similarly, a correction factor can be applied to the phantom-based path loss to obtain values that are more realistic (i.e., path loss values obtained from in vivo measurements). This correction factor as a function of distance and the corresponding mathematical expression are shown in Fig. 8.

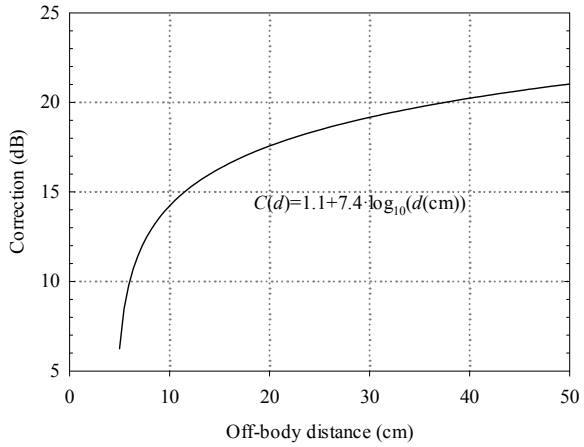

Fig. 8. Correction factor in decibels as a function of distance that can be applied to phantom-based measurements to fit *in vivo* measurements.

III. Conclusions

We have presented a set of path loss formulas, which are aimed to facilitate future research on the feasibility and design of deeply-implanted communication systems using ultra wideband signals. Some implantable biomedical applications, e.g., neural recording systems, have already been successfully demonstrated using ultra wideband interfaces [23]; however, in such applications the implantation depth rarely exceeds 3 centimeters. Our results provide a practical way to accurately estimate the path loss suffered by ultra wideband transmissions from wireless devices deeply implanted in the abdominal cavity for communication with an external unit. Although our path loss models are unavoidably antenna-dependent, they provide important insight into the behaviour of the most common implant channel scenarios. Our results can assist the biomedical engineer in the early stage of the design of wireless implantable sensors/actuators by evaluating accurately the feasibility of using an ultra wideband interface for a specific biomedical implantable application in the abdomen. With the correction factors that we provided, the biomedical engineer can perform channel measurements and transceiver tests in easy-to-build phantoms, and later adjust the results to values that are more realistic, thereby avoiding the complications of *in vivo* measurements.

References

[1] E. Jovanov and A. Milenkovic, "Body area networks for ubiquitous healthcare applications: opportunities and challenges," *Journal of Medical Sysems*, vol. 35, no. 5, pp. 1245-1254, Oct. 2011.

[2] *IEEE Standard for Local and Metropolitan Area Networks–Part 15.6: Wireless Body Area Networks*, IEEE Standard 802.15.6-2012, 2012.

[3] R. Chávez-Santiago and I. Balasingham, "Ultrawideband signals in medicine [Life Sciences]," *IEEE Signal Process. Mag.*, vol. 31, no. 6, pp. 130-136, Nov. 2014.

[4] E. Zastrow, S. K. Davis and S. C. Hagness, "Safety assessment of breast cancer detection via ultrawideband microwave radar operating in pulsed-radiation mode," *Microwave and Optical Technology Letters*, vol. 49, no. 1, pp. 221-225, Jan. 2007.

[5] R. Chávez-Santiago, K. Sayrafian-Pour, A. Khaleghi, K. Takizawa, J. Wang, I. Balasingham and H.-B. Li, "Propagation models for IEEE 802.15.6 standardization of implant communication in body area networks," *IEEE Commun. Mag.*, vol. 51, no. 8, pp. 80-87, Aug. 2013.

[6] A. Khaleghi, R. Chávez-Santiago and I. Balasingham, "Ultra-wideband pulse-based data communications for medical implants," *IET Communications*, vol. 4, no. 15, pp. 1189-1197, Oct. 2010.

[7] R. Chávez-Santiago, I. Balasingham, J. Bergsland, W. Zahid, K. Takizawa, R. Miura and H.-B. Li, "Experimental implant communication of high data rate video using an ultra wideband radio link," in *Proc. 35th Annual International Conference of the IEEE Engineering in Medicine & Biology Society (EMBC)*, Osaka, Japan, Jul. 3-7, 2013, pp. 5175-5178.

[8] K. M. S. Totahewa, J.-M. Redouté and M. S. Yuce, "A UWB wireless capsule endoscopy device," in *Proc. 36th Annual International Conference of the IEEE Engineering in Medicine & Biology Society (EMBC)*, Chicago, IL, Aug. 26-30, 2014, pp. 6977-6980.

[9] A. Daisuke, K. Katsu, R. Chávez-Santiago, Q. Wang, D. Plettemeier, J. Wang and I. Balasingham, "Experimental evaluation of implant UWB-IR transmission with living animal for body area networks," *IEEE Trans. Microw. Theory Techn.*, vol. 62, no. 1, pp. 183-192, Jan. 2014.

[10] J. Wang and Q. Wang, "Channel modeling and BER performance of an implant UWB body area link," in *Proc. 2nd International Symposium on Applied Sciences in Biomedical and Communication Technologies (ISABEL)*, Bratislava, Slovak Republic, Nov. 24–27, 2009, pp. 1-4.

[11] A. Khaleghi, R. Chávez-Santiago and I. Balasingham, "Ultra-wideband statistical propagation channel model for implant sensors in the human chest," *IET Microwaves, Antennas & Propagation*, vol. 5, no.15, pp. 1805-1812, Dec. 2011.

[12] A. Khaleghi, R. Chávez-Santiago and I. Balasingham, "An improved ultra wideband channel model including the frequency-dependent attenuation for in-body communications," in *Proc. 34th Annual International Conference of the IEEE Engineering in Medicine & Biology Society (EMBC)*, San Diego, CA, Aug. 28-Sep. 1, 2012, pp. 1631-1634.

[13] H. R. Bahrami, S. A. Mirbozorgi, L. A. Rusch and B. Gosselin, "Biological channel modeling and implantable UWB antenna design for neural recording systems," *IEEE Trans. Biomed. Eng.*, vol. 62, no.1, pp. 88-98, Jan. 2015.

[14] P. A. Floor, R. Chávez-Santiago, S. Brovoll, Ø. Aardal, J. Bergsland, O.-J. H. N. Grymyr, P. S. Halvorsen, R. Palomar, D. Plettemeier, S.-E. Hamran, T. A. Ramstad and I. Balasingham, "In-body to on-body ultra wideband propagation model derived from measurements in living animals," *IEEE J. Biomed. Health Inform.*, vol. 19, no. 3, pp. 938-948, May 2015.

[15] Q. Wang, K. Wolf and D. Plettemeier, "An UWB capsule endoscope antenna design for biomedical communications," in *Proc. 3rd International Symposium on Applied Sciences in Biomedical and Communication Technologies (ISABEL)*, Rome, Italy, Nov. 7-10, 2010, pp. 1-6.

[16] H. Yamamoto, J. Zhou and T. Kobayashi, "Ultra wideband electromagnetic phantoms for antennas and propagation studies," *IEICE Transactions on Fundamentals of Electronics, Communications and Computer Sciences*, vol. E91-A, no. 11, pp. 3173-3182, Nov. 2008.

[17] C. Tarín, P. Martí, L. Traver, N. Cardona, J. A. Díaz and E. Antonino, "UWB channel measurements for hand-portable devices: a comparative study," in *Proc. 18th Annual IEEE International Symposium on Personal, Indoor and Mobile Radio Communications (PIMRC)*, Athens, Greece, Sep. 3-7, 2007, pp. 1-5.

[18] C. Garcia-Pardo, R. Chávez-Santiago, N. Cardona and I. Balasingham, "Experimental UWB frequency analysis for implant communications," *2015 37th Annual International Conference of the IEEE Engineering in Medicine and Biology Society (EMBC)*, Milan, 2015, pp. 5457-5460.

[19] C. Gabriel, "Compilation of the Dielectric Properties of Body Tissues at RF and Microwave Frequencies," Brooks Air Force, N.AL/OE-TR-1996-0037, San Antonio, TX, 1996.

[20] A. Khaleghi and I. Balasingham, "Improving In-body Ultra Wideband Communications Using near-Field Coupling of the Implanted Antenna", *Microwave and Optical Technology Letters*, vol. 51, no. 3, pp. 585-589, March 2009.

[21] E. Y. Chow, Y. Ouyang, B. Beier, W. J. Chappell and P. P. Irazoqui, "Evaluation of cardiovascular stents as antennas for implantable wireless applications," *IEEE Trans. Microwave Theory Tech.*, vol. 57, no. 10, pp. 2523-2532, Oct. 2009.

[22] R. Chávez-Santiago, I. Balasingham, J. Bergsland, W. Zahid, K. Takizawa, R. Miura and H.-B. Li, "Experimental implant communication of high data rate video using an ultra wideband radio link," in *Proc. 35th Annual International Conference of the IEEE Engineering in Medicine & Biology Society (EMBC)*, Osaka, Japan, July 3-7, 2013, pp. 5175-5178.

[23] M. S. Chae, Z. Yang, M. R. Yuce, L. Hoang and W. Liu, "A 128-channel 6 mW wireless neural recording IC with spike feature extraction and UWB transmitter," *IEEE Trans. Neural Syst. Rehabil. Eng.*, vol. 17, no. 4, pp. 312-321, Aug. 2009.